



Effects of compaction state on structural strength of a clayey soil as determined by micropenetrometer tests

Qing Cheng^{1,2} · Chao-Sheng Tang² · De-Zheng Rong² · Hao-Da Li² · Bin Shi²

Received: 30 August 2022 / Accepted: 3 September 2023 / Published online: 24 September 2023
© The Author(s), under exclusive licence to Springer-Verlag GmbH Germany, part of Springer Nature 2023

Abstract

In this investigation, the structural strength of a clayey soil compacted at three different dry densities (1.7, 1.6 and 1.5 Mg/m³) and three different compaction water contents (20%, 16% and 12%) was studied by using a micropenetrometer. The penetration curves at various water contents during the drying and wetting cycle were analyzed. The maximum unit penetration strength and the penetration stiffness were used to represent the structural strength. Experimental results show that the structural strength increases with decreasing water content. At a given water content, the larger dry density, the larger structural strength and the smaller hysteresis loop induced by the drying-wetting cycle. At a higher dry density, the structural strength increases and the drying-wetting cycle induced hysteresis loop becomes smaller. Specimens compacted on the wet side of optimum water content exhibit a dispersed structure and those compacted on dry side of optimum water content have an aggregated structure. For soils with a dispersed structure, the structural strength increases with decreasing water content and the growth rate is gradually accelerated. However, for soils with an aggregated structure, when dried to water content lower than 8%, the structural strength increases by a small degree or even decreases. Moreover, the hysteresis loop of the soil specimens with dispersed structure is much smaller than those with an aggregated structure.

Keywords Compaction water content · Density · Microstructure · Penetration · Strength

1 Introduction

Compacted soils are widely used as a construction material. Therefore, strength characteristics of compacted soils are of great concern in geotechnical engineering and have been thoroughly investigated by performing different laboratory tests in the past decades (i.e., unconfined compressive strength tests, triaxial tests, direct shear tests, tensile strength tests, etc.). It is well-known that strength characteristics are the reflection of microscopic behavior of soils, which is governed by the arrangement of particles, aggregations of particles and the nature of particle contacts as well as distribution of soil pores and pore connectivity [5, 18, 19, 28]. The microstructure of compacted soils can be significantly affected by the compaction state including dry density and compaction water content [15, 20, 25, 34]. In terms of the density effects on soil microstructure, the most direct influence is that a larger dry density refers to a compression of soil pores and an increase in the contact of soil particles [6, 11, 35, 38]. With respect to the effect of compaction water content on soil microstructure, previous

✉ Chao-Sheng Tang
tangchaosheng@nju.edu.cn

Qing Cheng
chengqing@nju.edu.cn

De-Zheng Rong
rongdezheng@smail.nju.edu.cn

Hao-Da Li
haoda.li@smail.nju.edu.cn

Bin Shi
shibin@nju.edu.cn

¹ Key Laboratory of Geohazard Prevention and Geoenvironment Protection, Chengdu University of Technology, Chengdu 610059, China

² School of Earth Sciences and Engineering, Nanjing University, 163 Xianlin Road, Nanjing 210023, Jiangsu Province, China

researchers have found that a dispersed structure is developed in the soil specimen compacted on the wet side of the optimum water content as clay particles forming a matrix envelop the silt and fill the inter-granular voids. An aggregated structure is formed in the soil specimen compacted on the dry side of the optimum water content and both inter-aggregate pores and intra-aggregate pores can be observed [2, 5, 14, 26, 39, 41].

Micropenetrometer developed by Liu et al. [17] is to measure structural strength of soils, which is defined as the magnitude of intrusive force, with a certain probe, to break apart or pass through a microstructural unit of a soil. Using the micropenetrometer, Gu et al. [12] investigated the thermal effects on the structural strength of a clayey soil and found that structural strength decreased with increasing temperature. Wang et al. [33] studied the effects of wetting–drying cycles on the structural strength of a slurry specimen and found that the penetration curves change from mono-peak pattern to multi-peak pattern with increasing numbers of wetting–drying cycles. Tang et al. [30] compared the mechanical behavior of a saturated slurry specimen and an unsaturated compacted specimen by using the micropenetrometer. The previous studies all confirmed that the structural strength is sensitive to the change of soil water content. However, the structural strength of soil specimens with different microstructures induced by different compaction states as well as its response to water content are still unclear.

In this study, a series of micropenetrometer tests were conducted on a compacted clayey soil at different water contents during a drying and wetting cycle. The soil specimens were compacted at three different water contents (20%, 16% and 12%) and three different dry densities (1.7, 1.6 and 1.5 Mg/m³). The microstructure of the soil specimens was measured by using the mercury intrusion porosimetry (MIP). According to the obtained penetration curves during the drying and wetting cycle, the evolution of penetration strength and penetration stiffness of soil specimens with different compaction states were analyzed.

2 Materials and methods

2.1 Testing materials

The soil used in this study was collected from Nanjing, China. It is widely distributed in the middle and lower reaches of the Yangtze River. The mineralogical composition of the clay is mainly illite, followed by montmorillonite whereas its kaolinite content is very small. The fractions of sand, silt and clay are 2%, 76% and 22%, respectively. The liquid limit and plastic limit of the used soil are 36.5% and 19.5%, respectively. It is classified as a

lean clay (CL) according to the Unified Soil Classification System [1]. The index properties of the tested soil are summarized in Table 1.

2.2 Testing program and testing apparatus

In this study, two series of micropenetrometer test were carried out on soil specimens with various water contents during a drying and wetting cycle. In the first series, in order to investigate the density effect, micropenetrometer test was conducted on soil specimens with a compaction water content of 20%, but compacted at three different densities of 1.5, 1.6 and 1.7 Mg/m³. In order to investigate the effect of compaction water content, the second series of micropenetrometer tests were conducted on soil specimens with a density of 1.7 Mg/m³, but compacted at three different water contents of 12%, 16% (optimum water content) and 20%. Details of the testing program are listed in Table 2 and the water retention curves of each soil specimen are shown in Fig. 1.

A micropenetrometer [17] was used in this study to investigate the strength characteristics of the tested soil. Figure 2 shows a schematic diagram of this apparatus. During the penetration test, the prepared specimen is placed on the platen. The platen is driven by a motor and rises at a constant rate to allow the probe penetrate into the soil specimen. In this study, the penetration velocity of the probe is adjusted to be 2 mm/min. The penetration resistance is measured by a load transducer (with a capacity of 500 N and a resolution of 0.01 N) connected with the penetration probe, and the penetration depth is measured by a displacement transducer (with a capacity of 50 mm and a resolution of 0.01 mm) mounted on the platen. The penetration resistance and depth were measured at a time interval of 1.0 s. Note that the micropenetrometer was developed to measure structural strength inside soft soils,

Table 1 Index properties of the tested soil

Property	Value
Specific gravity	2.73
Sand content: %	2
Silt content: %	76
Clay content: %	22
Liquid limit: %	36.5
Plastic limit: %	19.5
Plastic index: %	17.0
Optimum water content: %	16.0
Maximum dry density: Mg/m ³	1.7

Table 2 Details of the testing program

Test ID	Compaction water content (%)	Dry density (Mg/m ³)	The applied drying-wetting cycle (percentages indicate soil gravimetric water content)
CW20D17	20	1.7	20% → 16% → 12% → 8% → 3% → 8% → 12% → 16% → 20%
CW20D16	20	1.6	
CW20D15	20	1.5	
CW16D17	16	1.7	16% → 12% → 8% → 3% → 8% → 12% → 16% → 20%
CW12D17	12	1.7	12% → 8% → 3% → 8% → 12% → 16% → 20%

the test results of soil samples with a low water content may be inaccurate but indicative.

Wetting of soil specimens was conducted using a designed wetting box, as shown in Fig. 3. A humidifier is used to generate the water mist. The de-aired water was then pumped into the chamber. Then, through a porous splitter, the atomized water was sprayed evenly onto the specimen. The soil specimen is placed on a shelf to prevent direct contact with water accumulated on the bottom. Note that the porous splitter is placed at a slight tilt to avoid condensation dripping onto the specimen.

2.3 Specimen preparation and testing procedure

The collected soil was air-dried, crushed and passed through a 2-mm sieve. Then, a certain amount of de-aired water was added to reach the target water contents of 20%, 16% and 12%, respectively. These mixtures were then sealed for 48 h for water to distribute uniformly. After that, static compaction with a fixed displacement rate of 0.4 mm/min was adopted to prepare compacted soil specimens to the target dry density (1.7, 1.6 and 1.5 Mg/m³) in an oedometer ring. The dimensions of the specimens are 61.8 mm in diameter and 40 mm in height. After compaction, the soil specimens were weighed immediately and then exposed to the temperature- and relative humidity-controlled laboratory environment for evaporation ($T = 30\text{ }^{\circ}\text{C}$, $\text{RH} = 45\%$). The soil specimens were dried to different water contents (16%, 12%, 8% and about 3% (fully air-dried)). When the soil specimen reached the target water content, it is sealed immediately for a 48-h curing. After curing, the specimens were taken for micropenetration test. Similar to the drying process, different target water contents (8%, 12%, 16% and 20%) were also set during the wetting path. The specimens were weighed at regular intervals and were taken out of the wetting equipment when the target water content is reached. The actual water content of each specimen is measured after the micropenetration test.

For the microstructure measurement, the soil specimens were cut into small cubes with a side length of about 5 mm and immersed into liquid nitrogen for a few minutes. Then,

the frozen specimens were put into a freeze-dryer for 48 h. After freeze-drying, the specimens were taken for MIP tests by applying an absolute pressure on mercury to enter the soil pores. The pore diameter can be calculated according to the Washburn equation [36].

3 Experimental results and discussion

3.1 Typical penetration curve in a micropenetrometer test

Figure 4a shows the penetration curves of soil specimens (compaction water content = 20%; dry density = 1.7 Mg/

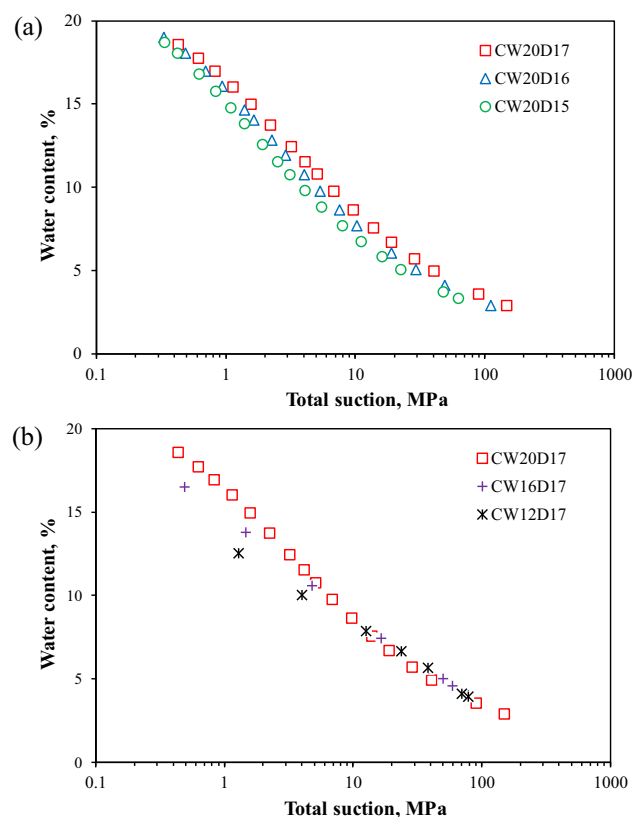


Fig. 1 Water retention curves of soil samples with different **a** dry densities and **b** compaction water contents

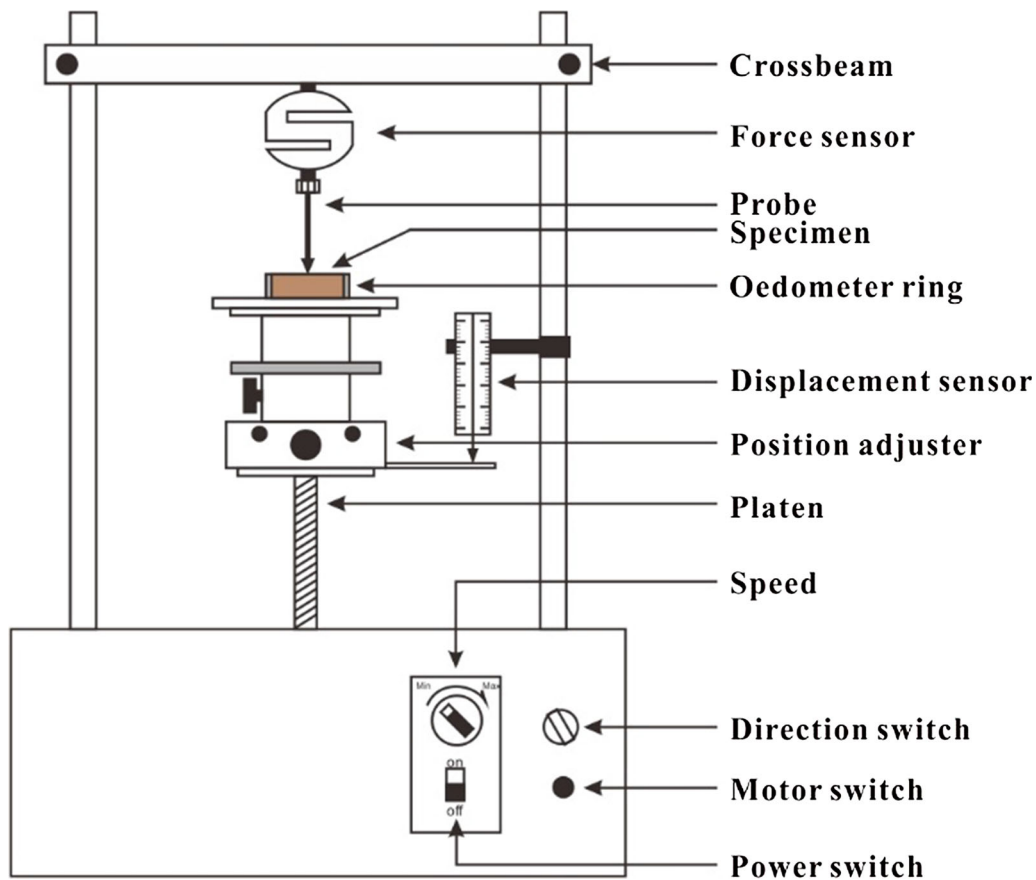


Fig. 2 Schematic diagram of the used micropenetrometer

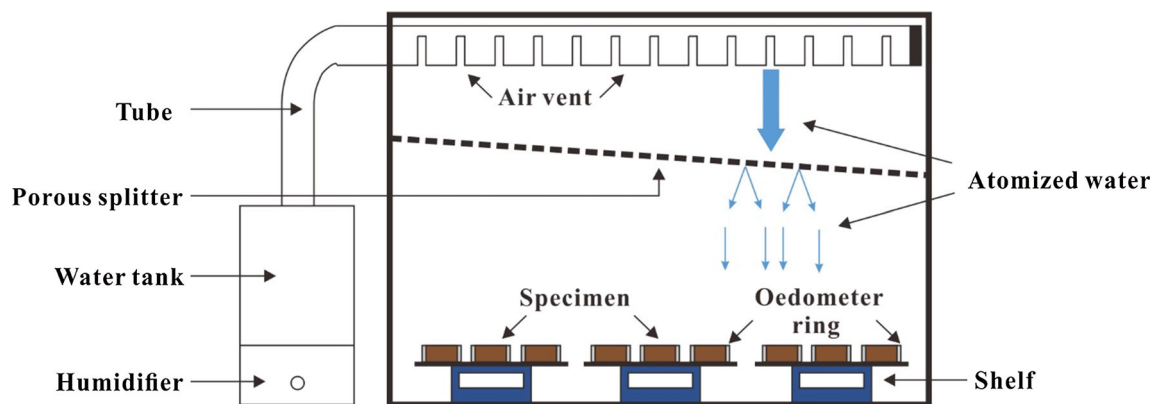


Fig. 3 Schematic diagram of the wetting equipment

m^3) with various water contents during the drying path. It can be seen from the figure that at a given water content, the penetration resistance increases almost linearly with increasing penetration depth at the early stage of the test. This is because a conical probe head was adopted in this study, the contact area between the probe and the soil specimen keeps increasing from the time the probe touches the soil to the time of full insertion [30, 33]. The penetration resistance initiates when the tip of the cone contacts

the specimen (as shown in Fig. 5a). A stress zone was generated around the contact area and two forces was applied onto the probe head: a frictional force f_s parallel to the contact surface and a compressive force N_s perpendicular to the surface. Both of these forces affect the penetration resistance of the soil specimen. As the probe continues to penetrate the soil, the increasing contact area between probe and soil creates larger stress zone (Fig. 5a, b). The compressive force N_s and surface friction f_s

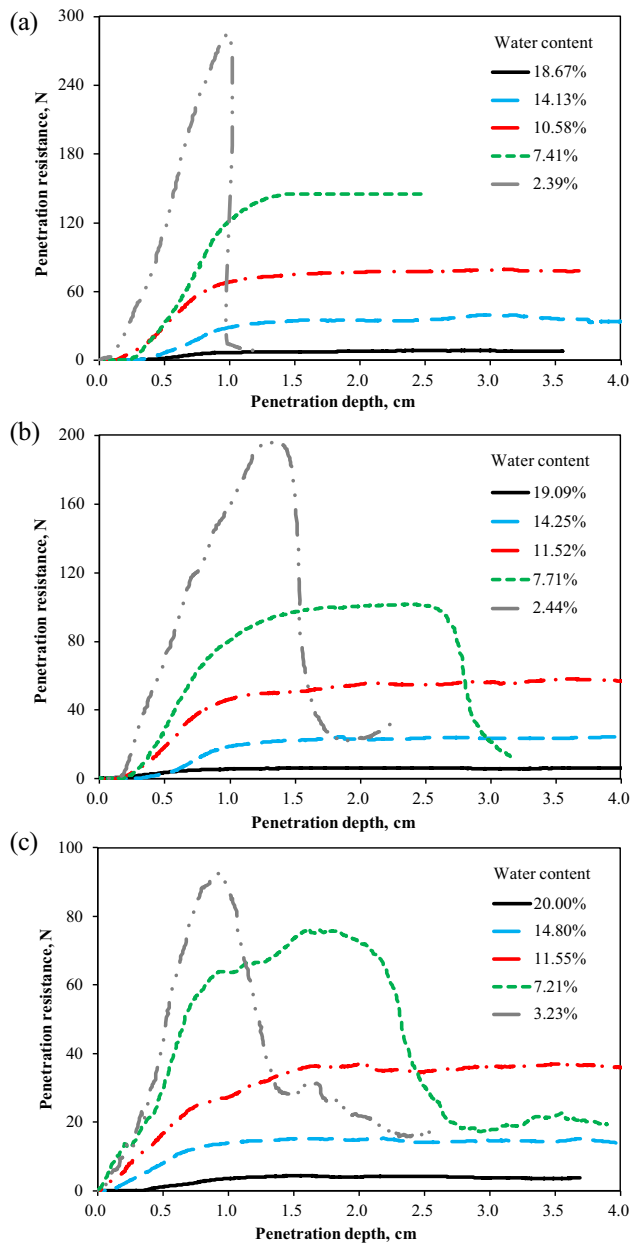


Fig. 4 Penetration curves of soil samples with three different dry densities during drying: **a** 1.7 Mg/m³; **b** 1.6 Mg/m³; **c** 1.5 Mg/m³

increase correspondingly. As a result, the penetration resistance increases monotonically with increasing penetration depth. As can be seen from the figure, a peak value generally appears at a penetration depth of around 1.0–1.5 cm. After reaching the peak value, the penetration resistance almost keeps constant with a small fluctuation. This happens when the conical probe head fully penetrates the soil. The size of the stress zone becomes stable (Fig. 5b, c). Both N_s and f_s reach equilibrium as the penetration continues. As a result, the penetration resistance will remain as a constant value, indicating good homogeneity in soil structure. As shown in Fig. 4a, most of

the soil specimens with various water contents show a similar pattern. However, for the soil specimen with an air-dried water content of about 3%, a sudden drop in penetration resistance can be found after reaching the peak value. This is likely because the soil specimen becomes brittle after air-drying. When the penetration probe comes into contact with the soil specimen, a local stress concentration occurs. Then, with gradually increasing pressure to a critical value, fracture occurs at this point. For the penetration curves of soil specimens with compaction water content of 20% and dry density of 1.6 and 1.5 Mg/m³, as shown in Figs. 4b and 3c, the trend is qualitatively similar.

3.2 Density effects on structural strength of a clayey soil

The maximum unit penetration strength can be obtained by using the peak value of the penetration resistance divided by the area of the probe head, which is a parameter intuitively representing the structural strength of soil specimen. Figure 6a illustrates the variation of maximum unit penetration strength of soil specimens with three different dry densities during the drying process. It can be seen that the maximum unit penetration strength increases with the decrease in water content during drying. This is because with decreasing water content, the soil suction increases and the stabilizing effect of suction on soil particles becomes more significant [8, 21, 37, 42]. Specifically, at the early stage of drying, the change of maximum unit penetration strength with decreasing water content is relatively slow. When water content decreases to 12%, a dramatic increase in maximum unit penetration strength can be observed. This is because suction in the lower water content range is more sensitive to changes in water content than that in the higher water content range [22]. At the compaction water content of 20%, the difference in maximum unit penetration strength between the three specimens with different dry densities is relatively small. During the drying process, at a given water content, the larger dry density, the larger maximum unit penetration strength. This is because a larger dry density leads to more contacts between soil aggregates and particles. When the water content decreases from 20 to 3%, for the soil specimen with a dry density of 1.7 Mg/m³, the maximum unit penetration strength increases from 2.8 to 94.8 MPa. While for the soil specimen with dry density of 1.6 and 1.5 Mg/m³, the maximum unit penetration strengths increase from 2.1 to 65.3 MPa and from 1.5 to 30.8 MPa, respectively. At the air-dried water content of about 3%, the maximum unit penetration strength of the soil specimens with dry density of 1.7 Mg/m³ (94.8 MPa) is over three times as large as that of the soil specimens with dry density of 1.5 Mg/m³ (30.8 MPa). The difference in maximum unit penetration

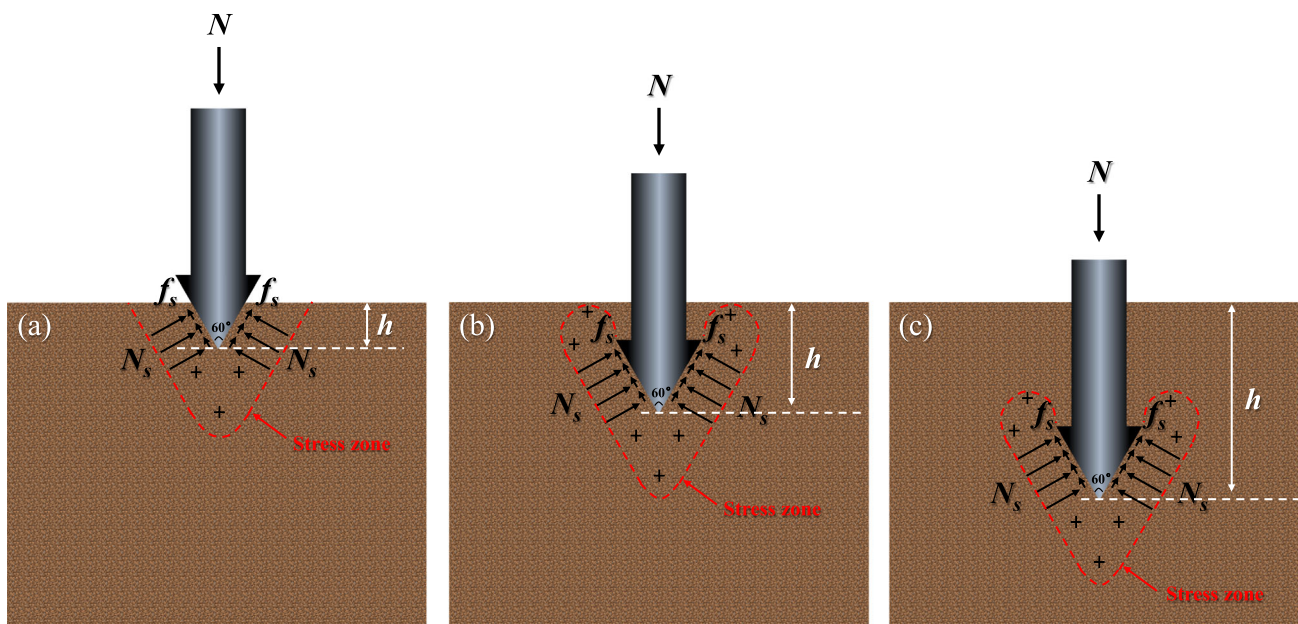


Fig. 5 Schematic drawing of the penetration process of the probe

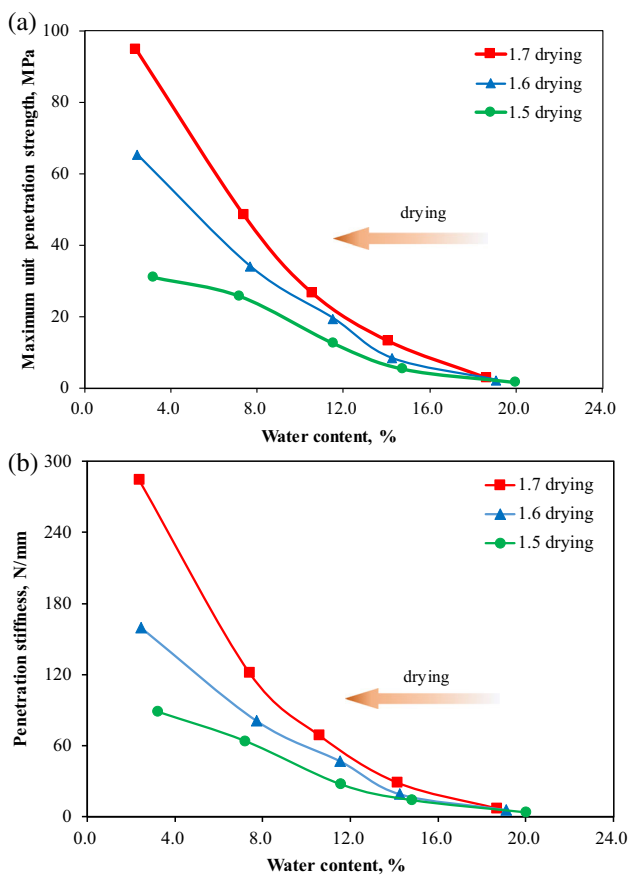


Fig. 6 Evolution of a maximum unit penetration strength and b penetration stiffness of soil samples with three different dry densities during drying

strength between the three specimens continues to increase with decreasing water content. As pointed by Gao et al. [10], in a wide range of water content, density effects on the evolution of strength induced by water content are insignificant. However, the contribution of water content to strength is not only the contribution of capillary force but also the effect of suction on soil dilatancy [23, 40], which may account for the observed phenomenon. In addition, stiffness is another important parameter to represent the structural characteristics of soil specimens. The slope of the penetration curve at the initial state can characterize the local soil stiffness. In this study, a penetration stiffness is defined as the slope of the penetration curve at the initial state with the penetration depth smaller than 1.0 cm. Figure 6b shows the evolution of penetration stiffness of soil specimens with three different dry densities during drying. As expected, as the water content decreases, the penetration stiffness of each soil specimen increases. When the water content decreases from 20 to 3%, the penetration stiffness of the three specimens with densities of 1.7, 1.6 and 1.5 Mg/m³ increases by 41, 28 and 24 times, respectively. Moreover, the influencing trend of dry density on structural strength investigated in this study is similar to that on macroscopic strength characteristics. Previous studies have shown that unsaturated soil with high dry densities demonstrates amplified shear strength, along with increased brittleness and enhanced stiffness [13, 19, 27, 31]. It proves that the structural strength can reflect the macroscopic mechanical behavior of soils.

Figure 7 shows the penetration curves of soil specimens with various water contents during the wetting path.

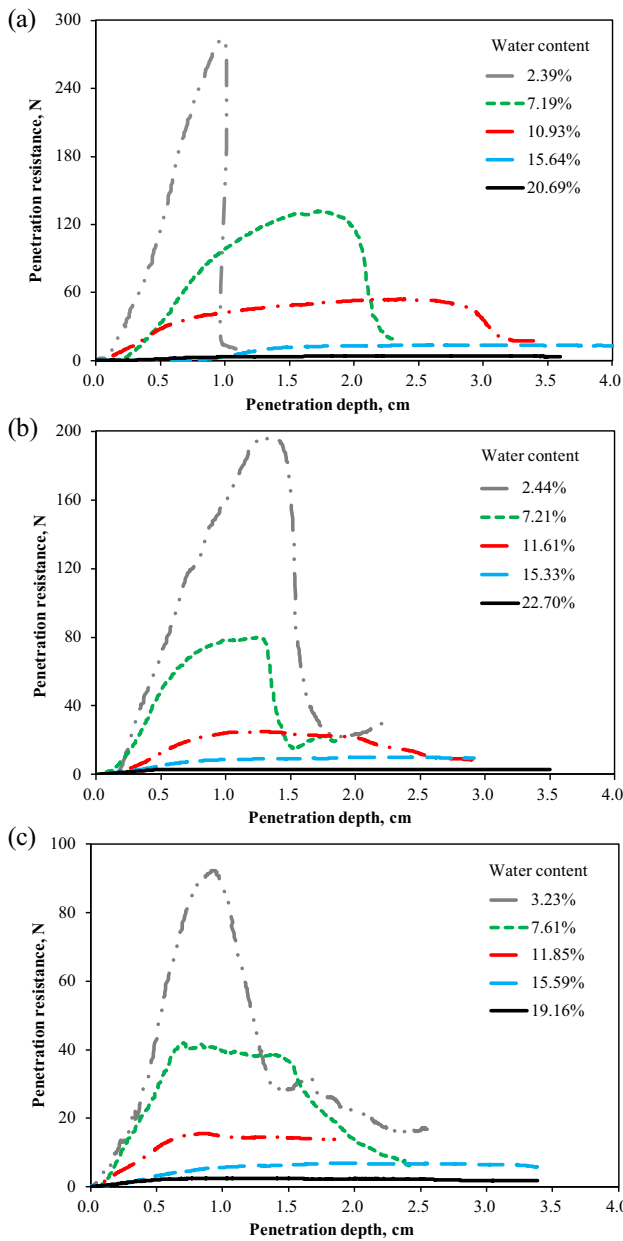


Fig. 7 Penetration curves of soil samples with three different dry densities during wetting: **a** 1.7 Mg/m³; **b** 1.6 Mg/m³; **c** 1.5 Mg/m³

Similarly, the maximum unit penetration resistance and the penetration stiffness of each soil specimen can be obtained from the figure. Figure 8 illustrates the evolutions of maximum unit penetration strength and penetration stiffness of soil specimens with three different dry densities during the drying and wetting cycle. For each soil specimen, at a given water content, the maximum unit penetration strength and penetration stiffness during the drying path is always larger than those during the wetting path. In other words, there is a hysteresis loop during the drying and wetting cycle for both maximum unit penetration strength and penetration stiffness. The hysteresis loop can be

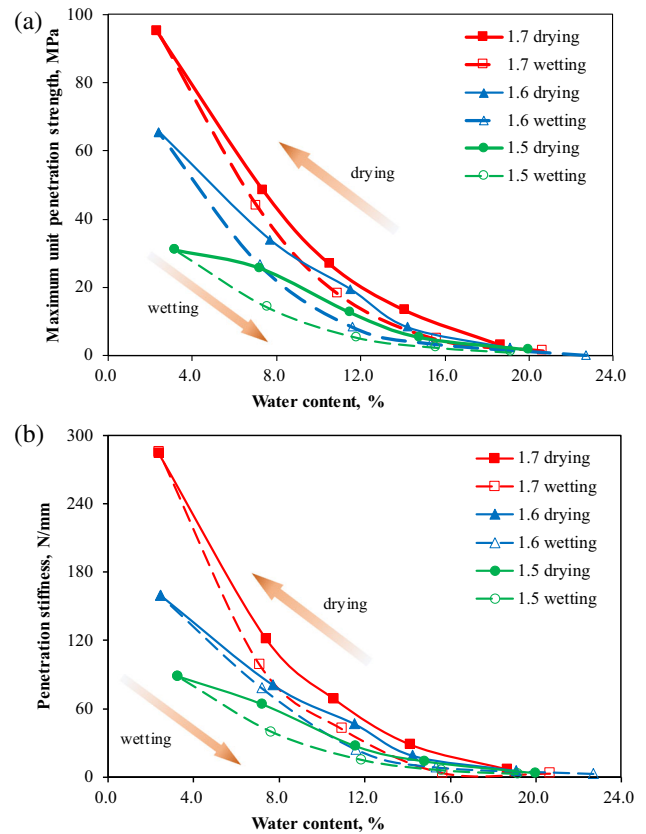


Fig. 8 Evolution of **a** maximum unit penetration strength and **b** penetration stiffness of soil samples with three different dry densities subjected to a drying-wetting cycle

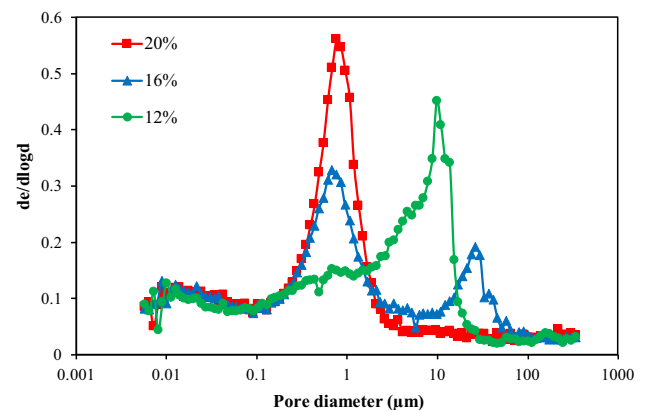


Fig. 9 Pore size distributions of the three soil samples compacted at various water contents of 20%, 16% and 12%

contributed by hydraulic hysteresis. At a given water content, the suction during the drying path is always larger than that during the wetting path [22]. The difference in surface tension induced by the difference in the contact angle at the receding soil–water interface during drying and at the advancing soil–water interface during wetting may also count. Moreover, it can be seen from the figure that the

size of the hysteresis loop becomes smaller as the dry density of soil specimen increases. This is because the average pore size of a soil specimen with a larger dry density is smaller and the corresponding difference in the receding and advancing contact angles is also smaller [24].

3.3 Effects of compaction water content on structural strength of a clayey soil

The pore size distributions of the soil specimens compacted at three different water contents of 20%, 16% and 12% are shown in Fig. 9. It can be found that for the soil specimen with a compaction water content of 20% (on the wet side of the optimum water content), a mono-modal pore size distribution is observed. This is attributed to the dispersed structure of the clay-particle matrix gathered around the silt grains [5]. The corresponding pore diameter at the peak point is about 0.9 μm . While for the soil specimen compacted at the optimum water content of 16%, a typical bi-modal pore size distribution is shown. Both inter-aggregate pores and intra-aggregate pores can be observed. This is due to an aggregate structure with clay particles assembling [5]. The corresponding pore diameters at the peak point of inter-aggregate pore and intra-aggregate pore are about 26.7 and 0.8 μm , respectively. Moreover, for the soil specimen with a compaction water content of 12% (on the dry side of the optimum water content), the bi-modal pore size distribution is not obvious. This phenomenon was also observed by Tarantino and De Col [32]. This is because with a decreasing compaction water content, the density function ($de/d\log d$) of intra-aggregate pore will decrease and that of inter-aggregate pore increases. As can be seen from the figure, the density function of inter-aggregate pore of the soil specimen with a compaction water content of 12% is much larger than that with a compaction water content of 16%.

By conducting the micropenetrometer tests on the soil specimens (compaction water content = 20%, 16% and 12%; dry density = 1.7 Mg/m^3) with various water contents during the drying path, the penetration curves can be obtained, as shown in Fig. 10. Based on these penetration curves, the maximum unit penetration resistance and the penetration stiffness of each soil specimen can be determined. Figure 11a illustrates the drying induced evolution of maximum unit penetration strength of soil specimens with three different compaction water contents. As expected, the maximum unit penetration strength increases with decreasing water content. For the soil specimen with a compaction water content of 20%, the increasing rate of maximum unit penetration strength with decreasing water content keeps increasing in the tested water content range. However, for the soil specimens compacted at water content of 16% and 12%, when dried to water content of about

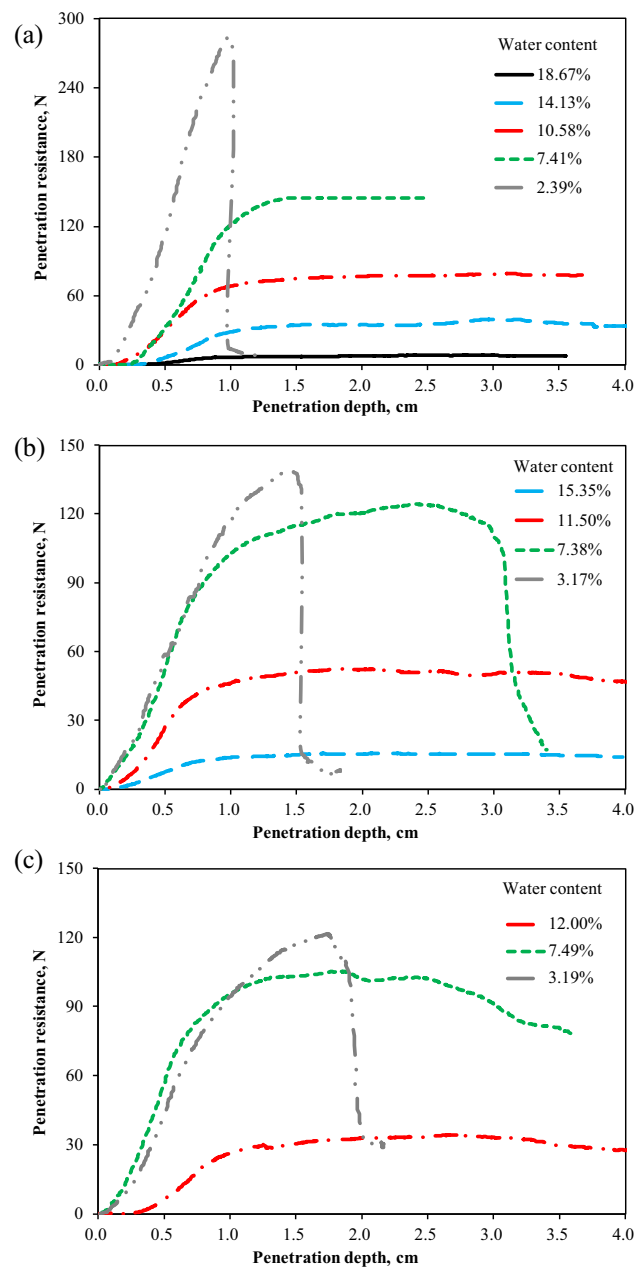


Fig. 10 Penetration curves during drying of soil samples compacted at various water contents: **a** 20%; **b** 16%; **c** 12%

8%, the increasing rate of maximum unit penetration strength suddenly diminishes to a very small value. The difference can be explained that for the soil specimens compacted on the wet side, there is no aggregation in the soil microstructure and suction is the most important factor controlling the soil behavior [41]. During the drying process, the decrease in water content leads to an increase in suction, resulting in an increase in the surface tension of the menisci water. As a result, the suction-induced normal force between soil particles increases, leading to an increase in the maximum unit penetration strength. For the

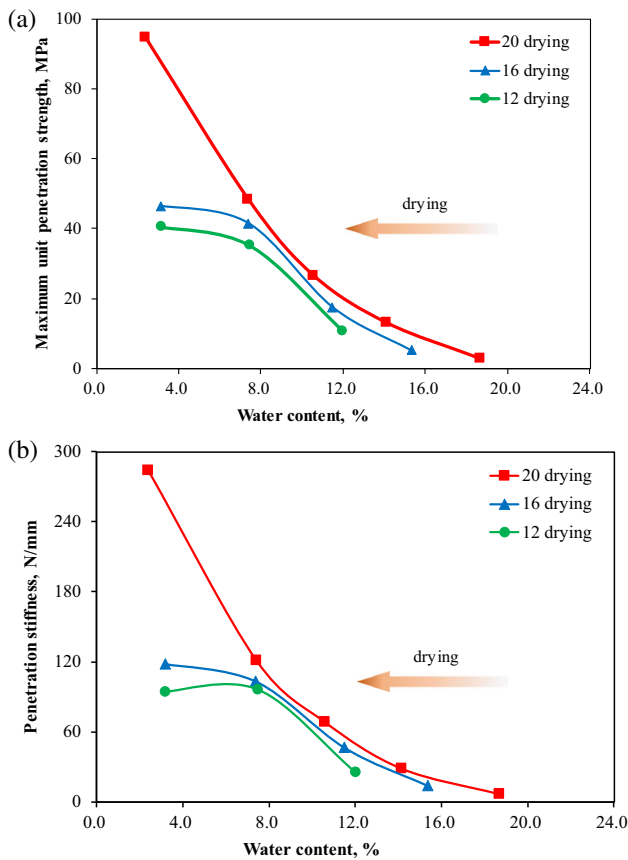


Fig. 11 Drying induced evolution of **a** maximum unit penetration strength and **b** penetration stiffness of soil samples with three different compaction water contents

soil specimens compacted on the dry side with an aggregated soil structure, both inter-aggregate pores and intra-aggregate pores exist in the soil microstructure and there is a pore diameter separating the two pore distinct. The delimiting pore diameter corresponds to a suction value and a water content value according to the Young–Laplace equation and the soil water retention curve. In the range of water content higher than the characteristic one, suction plays the most important role in soil behavior, similar to the previous discussion. While in the range of water content higher than the characteristic one, all the water in the inter-aggregate pores has been drained and the soil behavior is governed by the inter-aggregate contact, leading to a decrease in maximum unit penetration resistance with decreasing water content [41]. Based on the experimental results, it can be postulated that the specific value of the characteristic water content is around 8%.

Moreover, it can be found that in the tested range of water content, at a certain water content, the maximum unit penetration resistance of the soil specimen with a compaction water content of 20% is the largest, followed by that with a compaction water content of 16% and that with

a compaction water content of 12% is the smallest. This is likely because for the soil specimen compacted at water content of 20%, the average pore size is smaller than those compacted at water content of 16% and 12%, as shown in Fig. 9. A small pore diameter corresponds to a larger suction value and a larger inter-particle normal force. Thus, at a given water content, the maximum unit penetration resistance of the soil specimen with a dispersed structure is larger than that with an aggregated structure. Figure 11b shows the drying induced evolution of penetration stiffness of soil samples with three different compaction water contents. The variation tendency of penetration stiffness

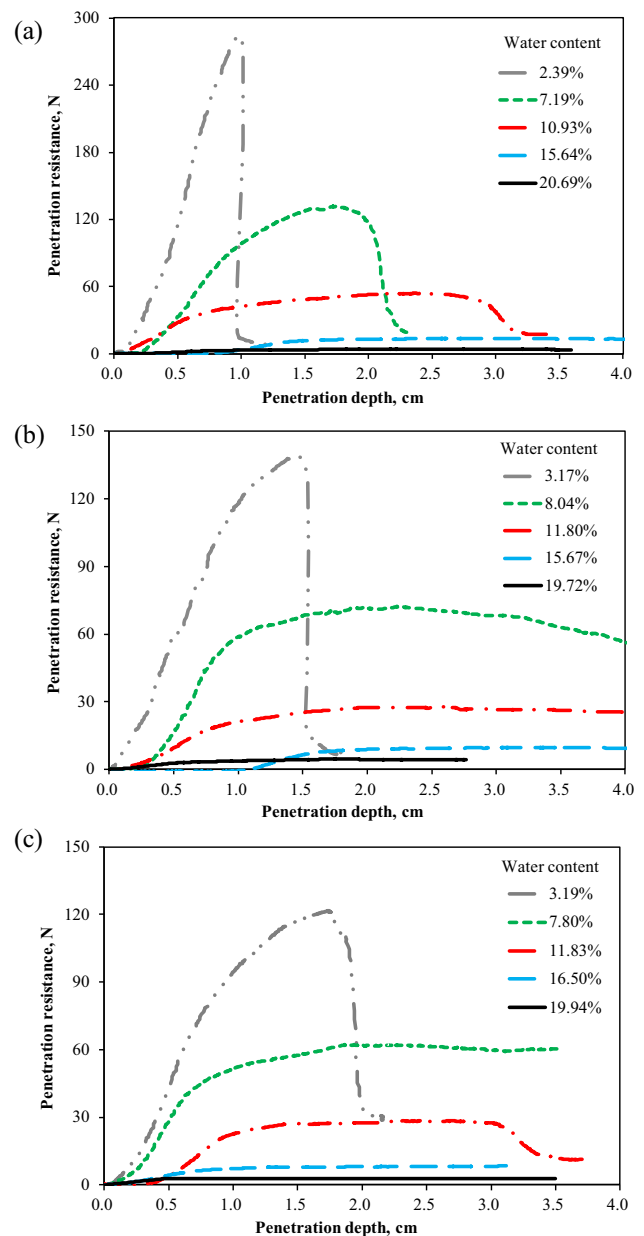


Fig. 12 Penetration curves during wetting of soil samples compacted at various water contents: **a** 20%; **b** 16%; **c** 12%

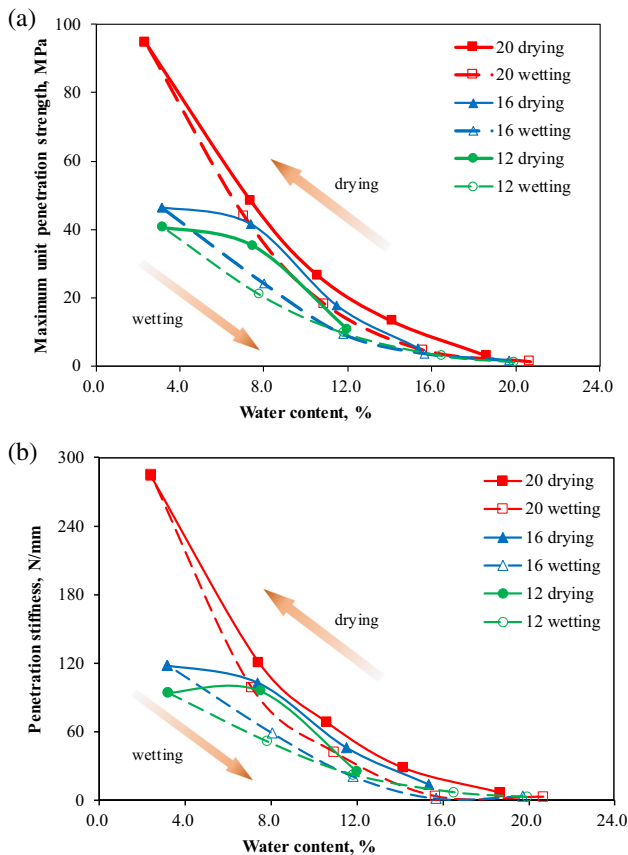


Fig. 13 Evolution of **a** maximum unit penetration strength and **b** penetration stiffness of soil samples compacted at three different water contents subjected to a drying-wetting cycle

with decreasing water content is similar to that of maximum unit penetration resistance shown in Fig. 11a. It should be noted that when drying from 8 to 3%, a decrease in penetration stiffness of the soil specimen with a compaction water content of 12% can be clearly observed, which is due to a reduction in inter-aggregate contact surface. Previous studies on the effects of compaction water content on the macroscopic strength characteristics of soils include both the effects of soil microstructure and the suction effect [4, 16, 31]. At the same water content, the difference in macroscopic strength characteristics of soil specimens with different microstructures induced by different compaction water content is not obvious. However, the difference in structural strength of soil specimens with different microstructures induced by different compaction water content is significant.

Figure 12 shows the penetration curves during wetting of soil samples compacted at various water contents of 20%, 16% and 12%. The determined maximum unit penetration strength and the penetration stiffness of each soil specimen are plotted in Fig. 13. The overall trend of the evolution of maximum unit penetration strength and the

penetration stiffness of soil specimens during the drying and wetting cycle has been analyzed in the previous section. The hysteresis loop can also be observed in both maximum unit penetration strength and penetration stiffness. Moreover, as can be seen from Fig. 13, the hysteresis loop of the soil specimen compacted at water content of 20% is much smaller than those compacted at water content of 16% and 12%. As discussed previously, the observed hysteresis loop is mainly due to the hydraulic hysteresis. For the soil specimen with a dispersed structure, the pore size distribution is more uniform compared to the soil specimen with an aggregated structure. Thus, the geometric non-uniformity of the individual pores in the soil specimen with a dispersed structure is less obvious, which is the main cause for the hydraulic hysteresis [3, 9, 24, 37]. Another possible reason is that the effect of drying-wetting cycle on the microstructural change of the soil specimen with an aggregated structure. As pointed by Romero et al. [29], the wetting path may lead to a soil structure dominated by bi-modal pore size distribution transferring to dominated by a single pore.

4 Conclusions

A micropenetrometer is used to investigate the effects of dry density and compaction water content on the structural strength of a clayey soil subjected to a drying and wetting cycle. In this study, the maximum unit penetration strength and the penetration stiffness are used to characterize the structural strength of a soil specimen with a given compaction state. The relationships between these two indices and water content were analyzed. The main outcomes of the study are summarized as follows:

(1) During the micropenetrometer test, typically the penetration resistance of a soil specimen first increases almost linearly with increasing penetration depth before reaching a peak point and then fluctuates in a small range. For the soil specimens with an air-dried water content of about 3%, the penetration resistance may drop after reaching the peak point as the specimen becomes brittle.

(2) The structural strength increases with decreasing water content because the stabilizing effect of suction on soil particles becomes more significant. The drying-wetting cycle results in a hysteresis loop in the structural strength, which is mainly due to the hydraulic hysteresis.

(3) With a larger dry density, both the maximum unit penetration strength and the penetration stiffness become larger as the contact area between soil particles is larger. While the drying-wetting cycle induced hysteresis loop is smaller because of a smaller average pore size distribution.

(4) For the soil specimen compacted at water content of 20% with a dispersed structure, the increasing rate of

structural strength with decreasing water content keeps increasing in the tested water content range. However, for the soil specimens compacted at water content of 16% and 12% with an aggregated structure, the increasing rate of structural strength increases at the early drying and suddenly diminishes to a small value when drying to the water content of about 8%. It even appears that the structural strength decreases. The hysteresis loop of the soil specimen with a dispersed structure is much smaller than those with an aggregated structure. This is because the geometric non-uniformity of the individual pores in the soil specimen with a dispersed structure is less obvious, leading to a smaller hydraulic hysteresis.

Acknowledgements This work was supported by the National Natural Science Foundation of China (Grant Nos. 42172290, 42230710, 41902271, 41925012), Natural Science Foundation of Jiangsu Province (Grant Nos. BK20221250, BK20211087), and the Fundamental Research Funds for the Central Universities.

Data availability Data are available on reasonable request.

References

- ASTM D-2487 (2017) Standard practice for classification of soils for engineering purposes (Unified Soil Classification System). American Society for Testing and Material, West Conshohocken
- Cheng Q, Tang CS, Zeng H, Zhu C, An N, Shi B (2020) Effects of microstructure on desiccation cracking of a compacted soil. *Eng Geol* 265:105418
- Cheng Q, Zhou C, Ng CWW, Tang CS (2019) A new water retention model that considers pore non-uniformity and evolution of pore size distribution. *Bull Eng Geol Environ* 78:5055–5065
- Çokça E, Erol O, Armangil F (2004) Effects of compaction moisture content on the shear strength of an unsaturated clay. *Geotech Geol Eng* 22:285–297
- Delage P, Audiguier M, Cui Y, Howat MD (1996) Microstructure of a compacted silt. *Can Geotech J* 33(1):150–158
- Delage P, Lefebvre G (1984) Study of the structure of a sensitive Champlain clay and of its evolution during consolidation. *Can Geotech J* 21(1):21–35
- Fisher R (1926) On the capillary forces in an ideal soil; correction of formulae given by W.B. Haines. *J Agric Sci* 16(3):492–505
- Gallipoli D, Gens A, Sharma R, Vaunat J (2003) An elasto-plastic model for unsaturated soil incorporating the effects of suction and degree of saturation on mechanical behaviour. *Géotechnique* 53(1):123–135
- Gao Y, Sun DA, Wu Y (2018) Hysteretic soil water characteristics and cyclic swell–shrink paths of compacted expansive soils. *Bull Eng Geol Environ* 77:837–848
- Gao Y, Sun DA, Zhu ZC, Xu YF (2019) Hydromechanical behavior of unsaturated soil with different initial densities over a wide suction range. *Acta Geotech* 14(2):417–428
- Griffiths FJ, Joshi RC (1989) Change in pore size distribution due to consolidation of clays. *Géotechnique* 39(1):159–167
- Gu K, Tang C, Shi B, Hong J, Jin F (2014) A study of the effect of temperature on the structural strength of a clayey soil using a micropenetrator. *Bull Eng Geol Environ* 73:747–758
- Guan GS, Rahardjo H, Choon LE (2010) Shear strength equations for unsaturated soil under drying and wetting. *J Geotech Geoenviron Eng* 136(4):594–606
- He Y, Cui YJ, Ye WM, Conil N (2017) Effects of wetting-drying cycles on the air permeability of compacted Teguline clay. *Eng Geol* 228:173–179
- Jiang Y, Chen WW, Wang GH, Sun GP, Zhang FY (2017) Influence of initial dry density and water content on the soil-water characteristic curve and suction stress of a reconstituted loess soil. *Bull Eng Geol Environ* 76(3):1085–1095
- Kong LW, Tan LR (2020) Study on shear strength and swelling-shrinkage characteristic of compacted expansive soil. In: *Unsaturated Soils for Asia*. CRC Press, pp 515–519
- Liu ZB, Shi B, Sheng DC (2006) A micropenetrator for detecting structural strength inside soft soils. *Geotech Test J* 29(6):443–450
- Marshall TJ, Holmes JW (1979) *Soil physics*. Cambridge University Press, Cambridge
- Mitchell JK, Soga K (2005) *Fundamentals of soil behaviour*, 3rd edn. Wiley, New Jersey
- Nowamooz H, Jahangir E, Masroufi F (2013) Volume change behaviour of a swelling soil compacted at different initial states. *Eng Geol* 153:25–34
- Ng CWW, Cheng Q, Zhou C (2018) Thermal effects on yielding and wetting-induced collapse of recomacted and intact loess. *Can Geotech J* 55(8):1095–1103
- Ng CWW, Menzies B (2007) *Advanced unsaturated soil mechanics and engineering*. Taylor & Francis, Milton Park
- Ng CWW, Mu QY, Zhou C (2016) Effects of soil structure on the shear behaviour of an unsaturated loess at different suctions and temperatures. *Can Geotech J* 54(2):270–279
- Ng CWW, Pang YW (2000) Experimental investigations of the soil-water characteristics of a volcanic soil. *Can Geotech J* 37:1252–1264
- Otalvaro IF, Neto MPC, Delage P, Caicedo B (2016) Relationship between soil structure and water retention properties in a residual compacted soil. *Eng Geol* 205:73–80
- Oualmakran M, Mercatoris BCN, Francois B (2016) Pore-size distribution of a compacted silty soil after compaction, saturation, and loading. *Can Geotech J* 53(12):1902–1909
- Rahardjo H, Melinda F, Leong EC, Rezaur RB (2011) Stiffness of a compacted residual soil. *Eng Geol* 120(1–4):60–67
- Romero E, Simms PH (2008) Microstructure investigation in unsaturated soils: a review with special attention to contribution of mercury intrusion porosimetry and environmental scanning electron microscopy. *Geotech Geol Eng* 26(6):705–727
- Romero E, Della Vecchia G, Jommi C (2011) An insight into the water retention properties of compacted clayey soils. *Géotechnique* 61(4):313–328
- Tang CS, Wang DY, Shi B, Li J (2016) Effect of wetting–drying cycles on profile mechanical behavior of soils with different initial conditions. *CATENA* 136:105–116
- Tang CS, Pei XJ, Wang DY, Shi B, Li J (2015) Tensile Strength of compacted clayey soil. *J Geotech Geoenviron Eng* 141(4):04014122
- Tarantino A, De Col E (2008) Compaction behaviour of clay. *Géotechnique* 58(3):199–213
- Wang DY, Tang CS, Cui YJ, Shi B, Li J (2016) Effects of wetting–drying cycles on soil strength profile of a silty clay in micro-penetrator tests. *Eng Geol* 206:60–70
- Wang Q, Cui YJ, Tang AM, Li XL, Ye WM (2014) Time- and density-dependent microstructure features of compacted bentonite. *Soils Found* 54(4):657–666
- Wang YH, Xu D (2007) Dual porosity and secondary consolidation. *J Geotech Geoenviron Eng ASCE* 133(7):793–801
- Washburn EW (1921) A note on a method of determining the distribution of pore sizes in a porous material. *Proc Natl Acad Sci USA* 7:115–116

37. Wheeler SJ, Sharma RS, Buisson MSR (2003) Coupling of hydraulic hysteresis and stress–strain behaviour in unsaturated soils. *Géotechnique* 53(1):41–54
38. Yu CY, Chow JK, Wang YH (2016) Pore-size changes and responses of kaolinite with different structures subject to consolidation and shearing. *Eng Geol* 202:122–131
39. Yuan SY, Liu XF, Buzzi O (2019) Effects of soil structure on the permeability of saturated Maryland clay. *Géotechnique* 69(1):72–78
40. Zhan LT, Ng CWW (2006) Shear strength characteristics of an unsaturated expansive clay. *Can Geotech J* 43(7):751–763
41. Zhang TW, Cui YJ, Lamas-Lopez F, Calon N, D’Aguiar SC (2018) Compacted soil behaviour through changes of density, suction, and stiffness of soils with remoulding water content. *Can Geotech J* 55(2):182–190
42. Zhou C, Ng CWW, Chen R (2015) A bounding surface plasticity model for unsaturated soil at small strains. *Int J Numer Anal Methods Geomech* 39(11):1141–1164

Publisher’s Note Springer Nature remains neutral with regard to jurisdictional claims in published maps and institutional affiliations.

Springer Nature or its licensor (e.g. a society or other partner) holds exclusive rights to this article under a publishing agreement with the author(s) or other rightsholder(s); author self-archiving of the accepted manuscript version of this article is solely governed by the terms of such publishing agreement and applicable law.